Lactobionic Acid-Modified Dendrimer-Entrapped Gold Nanoparticles for Targeted Computed Tomography Imaging of Human Hepatocellular Carcinoma

Hui Liu,[†,⊥] Han Wang,[‡,⊥] Yanhong Xu,[‡,⊥] Rui Guo,[†] Shihui Wen,[†] Yunpeng Huang,[†] Weina Liu,[†] Mingwu Shen,*[,†] Jinglong Zhao,[‡] Guixiang Zhang,*[,‡] and Xiangyang Shi*[,†,§]

[†]College of Chemistry, Chemical Engineering and Biotechnology, Donghua University, 2999 North Renmin Road, Shanghai 201620, P. R. China

[‡]Department of Radiology, Shanghai First People's Hospital, School of Medicine, Shanghai Jiaotong University, 100 Haining Road, Shanghai 200080, P. R. China

[§]CQM-Centro de Química da Madeira, Universidade da Madeira, Campus da Penteada, 9000-390 Funchal, Portugal

Ⓢ Supporting Information

ABSTRACT: Development of novel nanomaterial-based contrast agents for targeted computed tomography (CT) imaging of tumors still remains a great challenge. Here we describe a novel approach to fabricating lactobionic acid (LA)-modified dendrimer-entrapped gold nanoparticles (LA-Au DENPs) for in vitro and in vivo targeted CT imaging of human hepatocellular carcinoma. In this study, amine-terminated poly(amidoamine) dendrimers of generation 5 pre-modified with fluorescein isothiocyanate and poly(ethylene glycol)-linked LA were employed as templates to form Au nanoparticles. The remaining dendrimer terminal amines were subjected to an acetylation reaction to form LA-Au DENPs.

The prepared LA-Au DENPs were characterized via different methods. Our results reveal that the multifunctional Au DENPs with a Au core size of 2.7 nm have good stability under different pH (5−8) and temperature (4−50 °C) conditions and in different aqueous media, and are noncytotoxic to normal cells but cytotoxic to the targeted hepatocarcinoma cells in the given concentration range. In vitro flow cytometry data show that the LA-Au DENPs can be specifically uptaken by a model hepatocarcinoma cell line overexpressing asialoglycoprotein receptors through an active receptor-mediated targeting pathway. Importantly, the LA-Au DENPs can be used as a highly effective nanoprobe for specific CT imaging of hepatocarcinoma cells in vitro and the xenoplanted tumor model in vivo. The developed LA-Au DENPs with X-ray attenuation property greater than clinically employed iodine-based CT contrast agents hold a great promise to be used as a nanoprobe for targeted CT imaging of human hepatocellular carcinoma.

KEYWORDS: dendrimers, gold nanoparticles, CT imaging, hepatocellular carcinoma, lactobionic acid
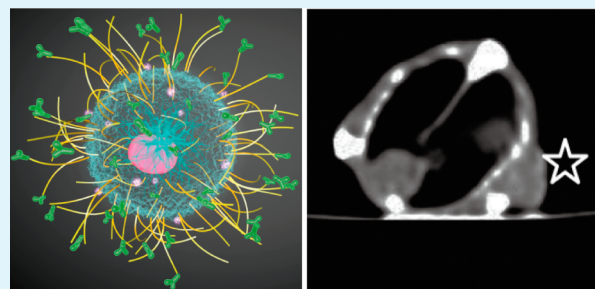
INTRODUCTION

Hepatocellular carcinoma (HCC) is the most common type of liver cancer with 700 000 cases diagnosed each year.[1,2] Most patients are diagnosed at a late stage, leading to difficulties to be cured. Therefore, early diagnosis using advanced technologies is essential. Molecular imaging has been emerging as a powerful tool to visualize, characterize, and quantify the biological process at the molecular and cellular levels in humans and other living systems.[3,4] As one of the mostly used molecular imaging technologies, computed tomography (CT) offers greater spatial and density resolution than other imaging modalities[5,6] and shows great potential in cancer diagnosis.[7−9] For high-quality and specific cancer CT imaging applications, contrast agents are usually indispensable. The clinically used iodinated contrast agents (e.g., Omnipaque) have severe drawbacks such as short circulation time, potential renal toxicity, and lack of targeting specificity.[10−14] Therefore, development of novel CT contrast agents that can overcome the above drawbacks is essential.

Various nanomaterial-based CT contrast agents, including but not limited to bismuth sulfide nanoparticles (NPs),[11,15,16] ytterbium-based NPs,[17] gold NPs (AuNPs),[7,8,12,18] and Gd-based complexes or NPs,[19,20] have been recently explored. In particular, AuNPs have received much attention due to the prolonged blood circulation time and greater CT imaging sensitivity than iodinated CT imaging agents (e.g., Omnipaque),[21−24] which are also shared by most of the other types of inorganic NPs. Besides, AuNPs are able to be easily synthesized, have good biocompatibility after appropriate

Scheme 1. Schematic Illustration of the Synthesis of LA-Au DENPs[a]
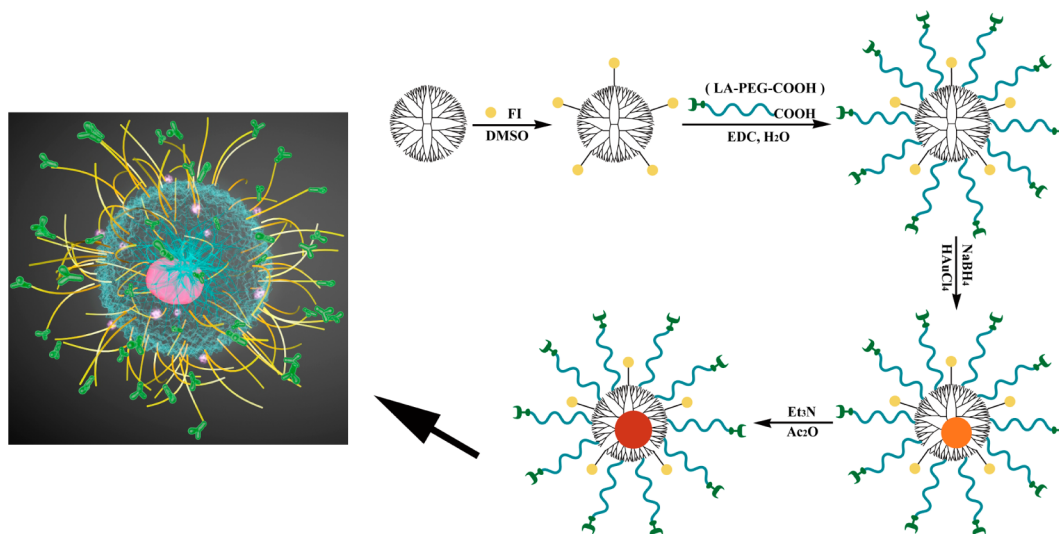
[a]Ac₂O and Et₃N represent acetic anhydride and triethylamine, respectively.

surface modification, and have the ability to be further functionalized.[7,9,10,18] These properties of AuNPs make them quite attractive to be used as CT contrast agents.[18,25,26]

Among the many polymer-based approaches to generating AuNPs,[27−34] dendrimer-mediated synthesis is versatile and allows for facile functionalization of the particle surfaces.[35−40] Dendrimers are a family of highly branched, monodispersed, synthetic macromolecules with well-defined composition, architecture, and abundant surface functional groups.[41,42] The unique structural characteristics of dendrimers enable the formation of dendrimer-entrapped AuNPs (Au DENPs)[8,10,25,26,39,43] as well as dendrimer-stabilized AuNPs (Au DSNPs)[21,36,44−46] for CT imaging applications. Our previous work has shown that generation 5 poly(amidoamine) (PAMAM) dendrimers with periphery modified by poly-(ethylene glycol) (PEG) can be used to entrap AuNPs for CT imaging applications.[8,25] By using G5 dendrimers modified with PEGylated folic acid (FA) as templates, multifunctional Au DENPs can be formed for targeted CT imaging of cancer cells and the xenografted tumor model overexpressing FA receptors.[39,47]

It is well known that asialoglycoprotein receptors (ASGPRs) are present on the surface of hepatocytes and several human carcinoma cell lines with a high density and show strong binding efficiency with galactose.[48,49] NPs modified with lactobionic acid (LA),[50] N-acetylgalactosamine,[51] and galactose[52] have been shown to be able to specifically bind to hepatocellular carcinoma cells (e.g., HepG2 cells). Another previous work has shown that LA-modified G5 dendrimers with terminal acetyl groups are able to effectively target human hepatocellular carcinoma in vitro.[50] Therefore, we expect that multifunctional LA-modified G5 dendrimers may be used as versatile templates to synthesize Au DENPs for targeted CT imaging of hepatocellular carcinoma in vitro and in vivo.

In this study, amine-terminated G5 PAMAM dendrimers (G5·NH₂) were first modified with fluorescein isothiocyanate (FI) and PEG-linked LA. The formed multifunctional G5 dendrimers were then employed as templates to form Au DENPs. Subsequent acetylation of the remaining surface amines of dendrimers led to the formation of multifunctional

LA-modified Au DENPs (LA-Au DENPs) with green fluorescent tags (Scheme 1). 3-(4,5-Dimethylthiazol-2-yl)-2,5-diphenyltetrazolium bromide (MTT) cell viability assay was used to assess the cytocompatibility of the probe. The targeting specificity of the probe was evaluated by flow cytometry assay of HepG2 cells in vitro. Finally, the multifunctional LA-Au DENPs were employed for CT imaging of HepG2 cells in vitro and the xenografted tumor model in vivo. To the best of our knowledge, this is the first report related to the use of LA-modified Au DENPs for targeted CT imaging of human hepatocellular carcinoma in vivo.

■ EXPERIMENTAL SECTION

Materials. Ethylenediamine core G5·NH₂ dendrimers having a polydispersity index smaller than 1.08 were supplied from Dendritech (Midland, MI). FI and LA were purchased from Aldrich. Chloroauric acid, acetic anhydride, and triethylamine were obtained from Sinopharm Chemical Reagent Co., Ltd (Shanghai, China). N-Hydroxysuccinimide (NHS) was from GL Biochem Ltd. (Shanghai, China). Dual functional PEG with both carboxyl and amine end groups (NH₂−PEG−COOH, M_w = 2000) and PEG monomethyl ether with carboxyl end group (mPEG−COOH, M_w = 2000) were obtained from Shanghai Yanyi Biotechnology Corporation (Shanghai, China). 1-Ethyl-3-(3-(dimethylamino)propyl) carbodiimide hydrochloride (EDC) was purchased from J&K Chemical Reagent Co., Ltd (Shanghai, China). Dialysis bags with molecular weight cut-off (MWCO) at 500 and 14 000 were from Shanghai Yuanye Biotechnology Corporation (Shanghai, China). HepG2 cells and L929 cells (a mouse fibroblast cell line) were from Institute of Biochemistry and Cell Biology, the Chinese Academy of Sciences (Shanghai, China). Mimimum essential medium (MEM), Dulbecco's modified eagle medium (DMEM), and fetal bovine serum (FBS) were purchased from Hangzhou Jinuo Biomedical Technology (Hangzhou, China) and Shanghai Excell Biology, Inc. (Shanghai, China), respectively. MTT was from Shanghai Sangon Biological Engineering Technology & Services Co., Ltd (Shanghai, China). Water used in all experiments was purified by using a Milli-Q Plus 185 water purification system (Millipore, Bedford, MA) with resistivity higher than 18.2 MΩ·cm.

Synthesis of Multifunctional FI- and LA-Modified G5 Dendrimers. In a typical synthesis, LA (78.45 μmol) was dissolved in NaH₂PO₄−Na₂HPO₄ buffer (pH = 6.0, 0.02 M, 5 mL) in the presence of equal molar equivalents of EDC and NHS under stirring. After 3 h, the activated LA (1.5 molar equiv) was dropwise added to

the NaH$_2$PO$_4$−Na$_2$HPO$_4$ buffer solution containing NH$_2$−PEG−COOH (52.30 μmol) under magnetic stirring for 3 days. The reaction mixture was then dialyzed against water (6 times, 2 L) using a dialysis membrane with MWCO of 500 for 2 days to remove the excess reactants, followed by lyophilization to obtain the product LA−PEG−COOH.

The synthesis of G5·NH$_2$−FI was carried out according to protocols illustrated in our previous work with slight modification.[37,53] In brief, FI solution (8.25 μmol in 1.726 mL of DMSO) was added into a solution of G5·NH$_2$ (1.65 μmol in 5 mL of DMSO) under magnetic stirring. After 24 h, the reaction mixture was extensively dialyzed against water (6 times, 2 L) using a dialysis bag with MWCO of 14 000 for 2 days to remove the excess reactants, followed by lyophilization to obtain the G5·NH$_2$−FI product.

The formed G5·NH$_2$−FI dendrimers were modified with LA−PEG−COOH via an EDC reaction. Briefly, LA−PEG−COOH (34.45 μmol in 5 mL of water) was first activated by five molar equivalents of EDC and NHS with vigorous stirring. After 3 h, the activated LA−PEG−COOH (18 molar equiv) was dropwise added to an aqueous solution of G5·NH$_2$−FI (1.91 μmol) under stirring. After 3 days, the reaction mixture was subjected to an extensive dialysis process against water (6 times, 2 L) using a dialysis membrane with MWCO of 14 000 for 2 days to remove the excess reactants, followed by lyophilization to obtain the product G5·NH$_2$−FI−PEG−LA.

Synthesis of Multifunctional LA-Modified Au DENPs. The formed G5·NH$_2$−FI−PEG−LA dendrimers were used as templates to form Au DENPs using sodium borohydride reduction chemistry with gold salt/dendrimer molar ratio at 150:1. Briefly, HAuCl$_4$ aqueous solution (154.50 μmol, 72.84 mM) was added into an aqueous solution of G5·NH$_2$−FI−PEG−LA (1.03 μmol, 55 mL) under magnetic stirring. Twenty minutes later, NaBH$_4$ solution (463.5 μmol, 170.13 mM in a mixed solvent of water/methanol, v/v = 2:1) with NaBH$_4$/HAuCl$_4$ molar ratio at 3:1 was added. The reaction mixture was stirred for 2 h. Then, the raw product of the Au DENPs was acetylated according to the literature.[3,21] In this context, triethylamine (134.5 μL), the raw Au DENP product (1.45 μmol, 80 mL), and acetic anhydride (76.1 μL) were used. The crude product was subjected to a similar dialysis and lyophilization process according to the literature[39] to get the $\{(Au^0)_{150}$−G5·NHAc−FI−PEG−LA$\}$ DENPs (LA-Au DENPs). Nontargeted $\{(Au^0)_{150}$−G5·NHAc−FI−mPEG$\}$ (nonLA-Au DENPs) were also prepared according to our previous report but with a Au salt/dendrimer molar ratio at 150:1 and with the same amount of FI moieties conjugated onto each dendrimer.[8]

Characterization Techniques. ^{1}H NMR spectrometry, UV-vis spectrometry, transmission electron microscopy (TEM), ζ-potential measurements, and dynamic light scattering (DLS) were used to characterize the formed particles. A detailed experimental procedure can be found in our previous work.[8,39,46] UV−vis spectroscopy was used to evaluate the stability of the LA-Au DENPs. The sample (0.2 mg mL^{-1}) was dispersed in water before measurements. The sample suspensions with a pH range of 5−8 and at different temperatures were prepared and measured according to protocols described in the literature.[46]

X-ray Attenuation Measurements. A CT imaging system (LightSpeed VCT, GE Medical Systems, Milwaukee, WI, USA) was used to measure the X-ray attenuation property of LA-Au DENPs. Details can be found in our previous work.[46]

Cell Culture. HepG2 cells and L929 cells were regularly cultured in MEM medium and DMEM medium, respectively, supplemented with 10% FBS and 1% penicillin-streptomycin at 37 °C and 5% CO$_2$.

Cytocompatibility Assay. MTT viability assay was performed to assess the cytocompatibility of LA-Au DENPs according to protocols described in our previous work.[46] Except the differences in the used cell lines, culture medium, and the concentration range of LA-Au DENPs (0−2000 nM), all the other procedures are similar.

Flow Cytometry. L929 or HepG2 cells were seeded in 24-well plates with a density of 2 × 10^5 cells/well. After overnight culture, the medium was exchanged with fresh medium containing the LA-Au DENPs with a concentration range of 0−1000 nM. For comparison,

nonLA-Au DENPs were also tested under similar experimental conditions. After 2 h incubation, the cells were washed with PBS 3 times, lifted via trypsinization, resuspended in 0.5 mL of PBS, and analyzed using a Becton Dickinson FACSCalibur flow cytometer.

In Vitro CT Imaging of Human Hepatocellular Carcinoma. HepG2 cells cultured and treated with LA-Au DENPs with different concentrations (200, 400, 600, 800, 1000, and 2000 nM, respectively) for 2 h were imaged using the same CT imaging system described above according to procedures described in our previous work.[46] NonLA-Au DENPs with the same concentrations were also tested for comparison.

In Vivo CT Imaging of the Tumor Model. All animal experiments were carried out according to the relevant laws and regulations and approved by the institutional ethical committee. Nude mice (20−25 g) were provided from Shanghai Slac Laboratory Animal Center (Shanghai, China). About 5.0 × 10^6 HepG2 cells were subcutaneously injected on the right back of each mouse. When the tumor volume reached about 1.2 cm^3 at 4 weeks post injection, each mouse was anesthetized according to an earlier report in our group.[46] LA-Au DENPs dispersed in PBS ([Au] = 0.1 M, 0.1 mL) were then intraperitoneally, intravenously, or intratumorally injected into mice. For comparison, nonLA-Au DENPs were also used to treat mice under similar conditions. The tumor-bearing mice were scanned using the above CT imaging system with tube voltage of 80 kV, tube current of 100 mA, and slice thickness of 0.625 mm. The in vivo biodistribution of the Au content within the major organs of heart, liver, spleen, lung, kidney, and tumor was quantified using inductively coupled plasma-optical emission spectroscopy (ICP-OES) (Leeman Prodigy, USA) at 2 h post-injection of the targeted and nontargeted Au DENPs following a similar mice treatment protocol described in our previous report.[39]

Statistical Analysis. Statistical analysis was carried out using the ANOVA statistical method according to an earlier report described by our group.[25]

■ RESULTS AND DISCUSSION

Synthesis and Characterization of LA-Au DENPs. Our earlier work has revealed that LA is able to be directly conjugated onto the surface of the dendrimer via an EDC coupling reaction.[50] In this study, a PEG spacer was employed to conjugate LA onto the dendrimer surface, which can not only improve the flexibility of the targeting ligand LA but also increase the periphery of dendrimers for enhanced loading of AuNPs.[8,25,39,47] The synthesis process and the structure of the final multifunctional Au DENPs are schematically illustrated in Scheme 1.

We first synthesized the PEG-linked LA (LA−PEG−COOH) and characterized it by ^{1}H NMR spectrometry (Figure S1a, Supporting Information). The peak at around 3.5 ppm attributed to PEG and the peaks in the range of 4.3−3.9 ppm assigned to LA clearly suggest the successful formation of the LA−PEG−COOH conjugate. Meanwhile, for flow cytometry analysis of cellular uptake of the Au DENPs with or without LA, FI was modified onto the dendrimer surface to form the G5·NH$_2$−FI conjugate. This can also be confirmed by ^{1}H NMR (Figure S1b, Supporting Information). By comparison of the integrated area of the NMR peaks associated with FI (6−8 ppm) and the NMR peaks of the dendrimer −CH$_2$− protons, the number of FI moieties attached to each dendrimer was measured to be 5.3. Then, we modified LA−PEG−COOH onto the G5·NH$_2$−FI dendrimer surface via an EDC reaction to form the G5·NH$_2$−FI−PEG−LA conjugate. Similarly, through the NMR peak integration, the number of LA−PEG moieties attached onto each G5 dendrimer was estimated to be 10.8 (Figure S1c, Supporting Information).
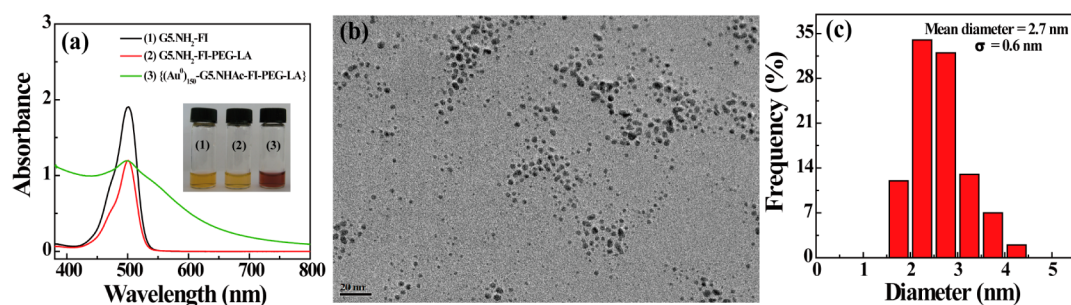
Figure 1. (a) UV−vis spectra of the synthesized G5·NH$_2$−FI (1), G5·NH$_2$−FI−PEG−LA (2), and LA-Au DENPs (3). (b) TEM image and (c) size distribution histogram of the formed LA-Au DENPs. The inset of (a) shows the photograph of the solutions of G5·NH$_2$−FI (1), G5·NH$_2$−FI−PEG−LA (2), and LA-Au DENPs (3).

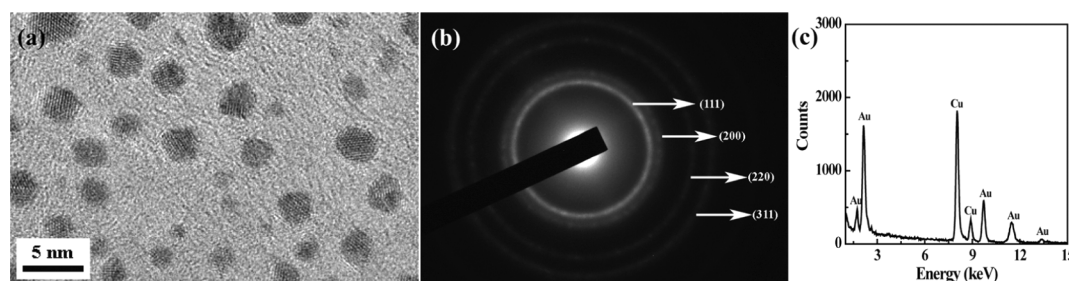**Figure 2.** Typical high-resolution TEM image (a), SAED pattern (b), and EDS spectrum (c) of the LA-Au DENPs.

We then used the formed G5·NH$_2$−FI−PEG−LA dendrimers as templates to generate AuNPs. The selection of the Au salt/dendrimer molar ratio at 150:1 is based on the balance of the stability of the products and the effort to improve the CT imaging sensitivity. In principle, higher CT imaging sensitivity can be achieved when more Au content was entrapped within the dendrimer. When the Au salt/dendrimer molar ratio excesses a certain threshold, the NPs become unstable. The last step of acetylation is key to neutralize the surface positive potential of the formed LA-Au DENPs, which is important to avoid their nonspecific binding with negatively charged cell surfaces and to improve the cytocompatibility of the particles.[36,37,54,55] The emergence of the proton signal at 1.87 ppm associated with the −CH$_3$ protons of the acetamide groups in the ^{1}H NMR spectrum (Figure S1d, Supporting Information) clearly indicates the transformation of dendrimer remaining terminal amines to acetamide groups. It should be noted that under the given experimental conditions the hydroxyl groups of LA are not able to be acetylated, which can be confirmed by the NMR spectra. We also note that peaks b and c shown in Figure S1a disappear in Figure S1(c, d), and peaks f, d, and e shown in Figure S1(b, c) disappear in Figure S 1d. This is possibly ascribed to the insensitivity of the NMR technique. The samples with the same modified molecular segments but with different scales (the different molar amounts of the same molecular segments) may not be exactly identified in a similar manner. Further ζ-potential measurements show that the formed LA-Au DENPs display a nearly neutral surface potential (3.7 ± 0.7 mV), demonstrating the success of the acetylation reaction. In contrast, the LA-Au DENPs before acetylation have a quite positive surface potential (26.9 ± 1.0 mV).

UV−vis spectrometry and TEM were used to characterize the formed LA-Au DENPs (Figure 1). Both G5·NH$_2$−FI and G5·NH$_2$−FI−PEG−LA dendrimers display a typical absorption peak at 500 nm, which can be assigned to the contribution of the attached FI moiety.[53] After the formation of Au DENPs, a strong build-up appeared in the range of 500−800 nm, which is typically attributed to the NP-resulted light-scattering effect. The shoulder in the range of 500−550 nm should be related to the overlapping of the surface plasmon resonance (SPR) band of AuNPs and the FI absorbance peak. The formation of Au DENPs was also visually confirmed by the solution color change from yellow to wine red, which is the typical color of colloidal AuNPs (Figure 1a, inset). The formed LA-Au DENPs were characterized by TEM imaging (Figure 1b and 1c), revealing that the particles are spherical or semispherical in shape and have a fairly narrow size distribution with a mean diameter of 2.7 ± 0.6 nm. Further DLS measurements reveal that the hydrodynamic size of the LA-Au DENPs is 343.8 ± 38.0 nm with a polydispersity index of 0.631 ± 0.075. It is interesting to note that the measured hydrodynamic size of LA-Au DENPs is much bigger than that measured by TEM. This is presumably due to the fact that TEM measures single Au core NPs, while DLS measures the Au DENPs in a clustered state in aqueous solution which is likely to be composed of a lot of Au DENPs, corroborating our previous results.[21,46,56] Similarly, UV−vis spectrometry and TEM were also used to characterize the nonLA-Au DENPs (Figure S2, Supporting Information). The pretty much similar particle size and size distribution validate the effective comparison in terms of the LA-mediated targeting efficacy.

The crystalline structure of the LA-Au DENPs was characterized by TEM technologies (Figure 2). The high-resolution TEM image clearly shows the lattices of the AuNPs (Figure 2a). In addition, the selected area electron diffraction (SAED) pattern of the AuNPs confirmed the face-centered-cubic (fcc) crystal structures of the formed particles via the observation of the (111), (200), (220), and (311) rings (Figure 2b). The existence of the Au element was further confirmed by energy-dispersive spectroscopy (Figure 2c).
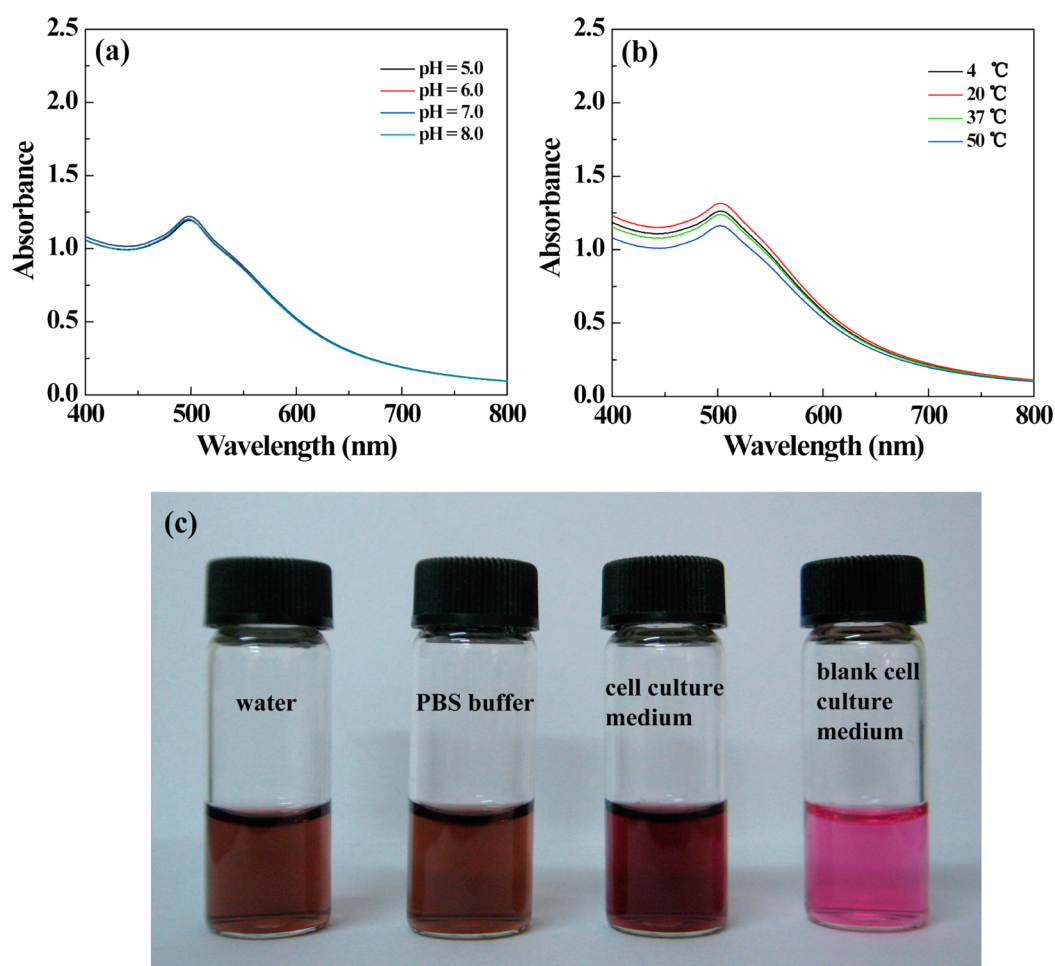
Figure 3. UV-vis spectra of LA-Au DENPs under different pH (a) and temperature (b) conditions. The photograph of the as-prepared LA-Au DENPs dispersed in different aqueous media for one month (c).
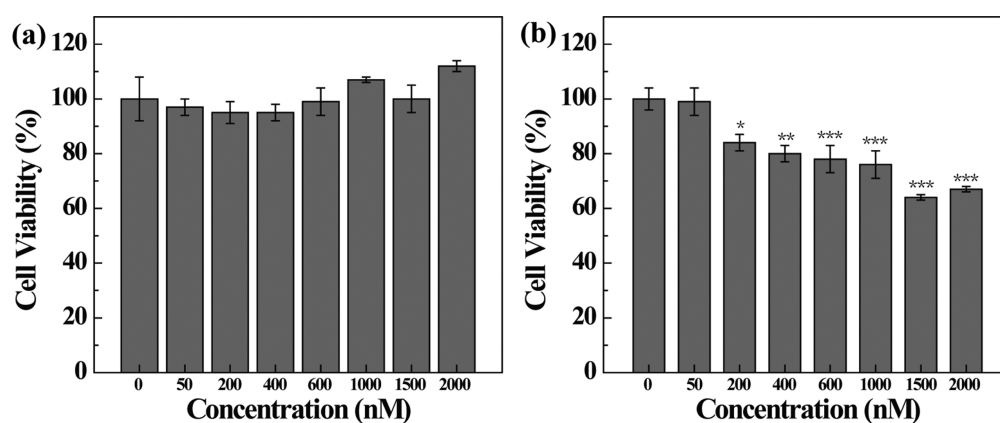

Figure 4. MTT assay of L929 (a) and HepG2 (b) cell viability after treatment with LA-Au DENPs for 24 h. The cells treated with PBS buffer were used as control. The data were expressed as mean ± S.D ($n = 4$).

UV−vis spectroscopy was used to evaluate the colloidal stability of the LA-Au DENPs (Figure 3), similar to our previous studies.[21,26] UV−vis spectra of LA-Au DENPs dispersed in water with different pHs (pH = 5−8, Figure 3a) at room temperature (20 °C) and the particles exposed to water at the temperatures of 4, 20, 37, and 50 °C, respectively (Figure 3b), reveal that the SPR peak-associated shoulder band of the NPs does not have any significant changes. We further evaluated the colloidal stability of the LA-Au DENPs by

dispersing the particles in water, PBS, and cell culture medium, respectively, for one month (Figure 3c). The particles do not precipitate at room temperature. The stability of the LA-Au DENPs dispersed in PBS was also occasionally checked by DLS. We show that the hydrodynamic size of the particles does not change significantly for at least 1 week. Taken together, the formed LA-Au DENPs have good stability under the given pH and temperature conditions and in varying water-based media.
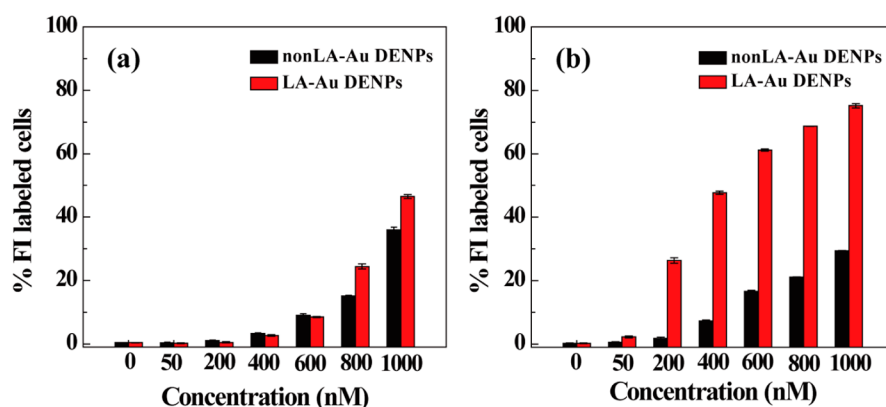
Figure 5. Flow cytometry analysis of L929 (a) and HepG2 (b) cells after treatment with Au DENPs with or without modification of LA for 2 h. The cells treated with PBS buffer were used as control.

Cytotoxicity Assay. The cytotoxicity of the LA-Au DENPs was then investigated via MTT cell viability analysis (Figure 4). Both L929 and HepG2 cells were used for the tests. For the normal L929 cells, it seems that the cell viability does not change at the particle concentration ranging from 0 to 2000 nM, suggesting the good cytocompatibility of the LA-Au DENPs in the given concentration range (Figure 4a). However, in the case of HepG2 cells, the cell viability decreases to some extent with the increase of LA-Au DENP concentration (Figure 4b). This difference should be attributed to cell-type-associated cellular uptake of the LA-Au DENPs. The presence of ASGPR on the surface of HepG2 cells may enable enhanced cellular uptake of LA-Au DENPs via a receptor-mediated pathway, thereby leading to the viability decrease of the HepG2 cells, especially at the higher concentrations (1500 and 2000 nM). In contrast, L929 cells without ASGPR on their surface do not seem to have significant uptake of the particles, and consequently in the studied concentration range, LA-Au DENPs do not significantly impact the cell viability.

Flow Cytometry. The targeted cellular uptake of FI-labeled Au DENPs with or without LA was further evaluated by flow cytometry (Figure 5a and Figure S3, Supporting Information). We can clearly see that both Au DENPs with or without LA have increased uptake in L929 cells with the particle concentration, and there is no obvious difference between nonLA-Au DENPs and LA-Au DENPs under similar concentrations. This could be due to the fact that the cellular uptake of both particles is primarily via concentration-dependent phagocytosis and/or cell membrane diffusion mechanisms,[8,22] and the LA modification on the surface of Au DENPs does not play a significant role.

In sharp contrast, when HepG2 cells were incubated with LA-Au DENPs or nonLA-Au DENPs, the binding affinity of the two particles is significantly different at the particle concentration of 200 nM or above (Figure 5b and Figure S4, Supporting Information). The much higher uptake of LA-Au DENPs than that of nonLA-Au DENPs under similar particle concentrations should be ascribed to the LA-mediated targeting to HepG2 cells overexpressing ASGPR. In this case, the nonspecific cellular uptake mechanisms (phagocytosis and diffusion via cell walls) also applied to both particles with or without LA; therefore, both particles had increased uptake in the cells with the particle concentration.

X-ray Attenuation Measurements. We then investigated the X-ray attenuation property of the formed LA-Au DENPs (Figure 6). Omnipaque was used as control. We show that the
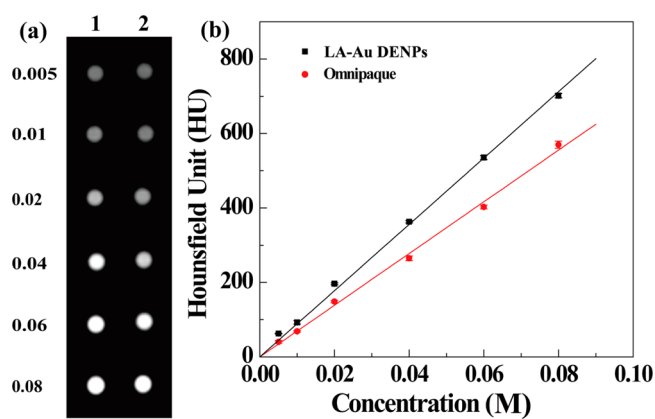

Figure 6. (a) CT images of (1) LA-Au DENPs and (2) Omnipaque with different concentrations. (b) X-ray attenuation intensity (HU) of LA-Au DENPs and Omnipaque as a function of the molar concentration of the active element (Au or iodine). In (a), the numbers on the left represent the Au or iodine concentration (M) of the particles or Omnipaque.

CT image brightness increases with the particle concentration for the LA-Au DENPs, similar to the case of Omnipaque (Figure 6a). At the Au or iodine concentration of 0.02 M or above, the CT image of the LA-Au DENPs is much brighter than those of Omnipaque under similar radiodense element concentrations. Further quantitative analysis data reveal that the X-ray attenuation intensity of both LA-Au DENPs and Omnipaque increases with the molar concentration of the radiodense element of Au or iodine (Figure 6b). However, the LA-Au DENPs display much higher X-ray attenuation intensity than Omnipaque under similar radiodense element concentrations (0.04 M or above). The better X-ray attenuation property of LA-Au DENPs than that of Omnipaque is crucial for more sensitive CT imaging applications.

In Vitro Cancer Cell CT Imaging. We next used LA-Au DENPs for targeted CT imaging of HepG2 cells in vitro. NonLA-Au DENPs without LA modification were also tested for comparison. Quantification of the cell CT values (Figure 7) reveals that the CT value of HepG2 cells increases with the concentration of Au DENPs with or without LA, and higher particle concentration results in higher cell CT values. Compared to nonLA-Au DENPs, the HepG2 cells treated with LA-Au DENPs show more significant CT contrast enhancement at the same corresponding particle concen-
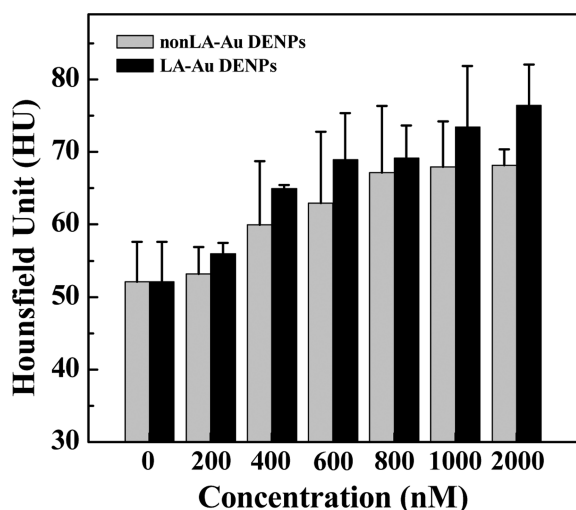
Figure 7. CT values of the HepG2 cells treated with nonLA-Au DENPs and LA-Au DENPs as a function of particle concentration.

trations (200 nM or above), which is likely ascribed to the LA-mediated specific binding and cellular uptake of the particles.

In Vivo CT Imaging of the Xenografted Tumor Model.
The possibility to employ LA-Au DENPs as a probe for targeted CT imaging of a xenoplanted HepG2 tumor model in vivo was then tested. To achieve the better tumor CT imaging performance, both intravenous and intraperitoneal injection routes were used to deliver the particles to the mice. Shown in Figure 8 are the respective CT images of tumors before and after respective intravenous and intraperitoneal administration of LA-Au DENPs. NonLA-Au DENPs without LA were also injected into other tumor mice for comparison. It is interesting to note that the tumor size in different mice is quite similar, which ensures reasonable comparison and evaluation of CT imaging contrast enhancement. The difference of the tumor size shown in the CT images is attributed to the different planes in the scanned images.

Due to the difficulty to visually differentiate the CT image brightness of the tumor sites,[44] it is essential to quantify the CT signal intensity via the manufacturer's standard display program (Figure 9). For the nontargeted group (nonLA-Au DENPs), the tumor CT value gradually increases after injection, and all CT values are much higher than that before injection. This enhancement may be ascribed to the known EPR effect, allowing for passive accumulation of the nonLA-Au DENPs in the tumor region. The tumor CT values of the targeted group
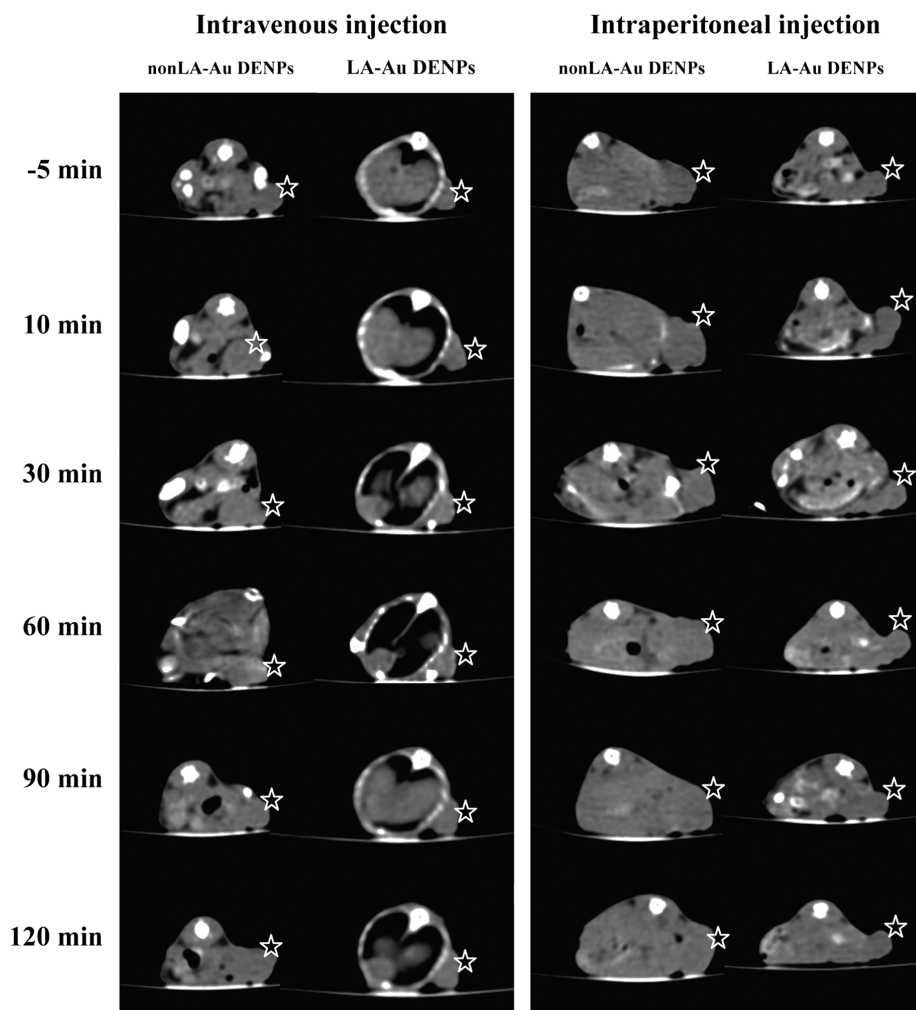

Figure 8. CT images of the xenografted HepG2 tumor model before and after intravenous or intraperitoneal injection of nonLA-Au DENPs and LA-Au DENPs at different time points post injection. The stars indicate the tumor area.
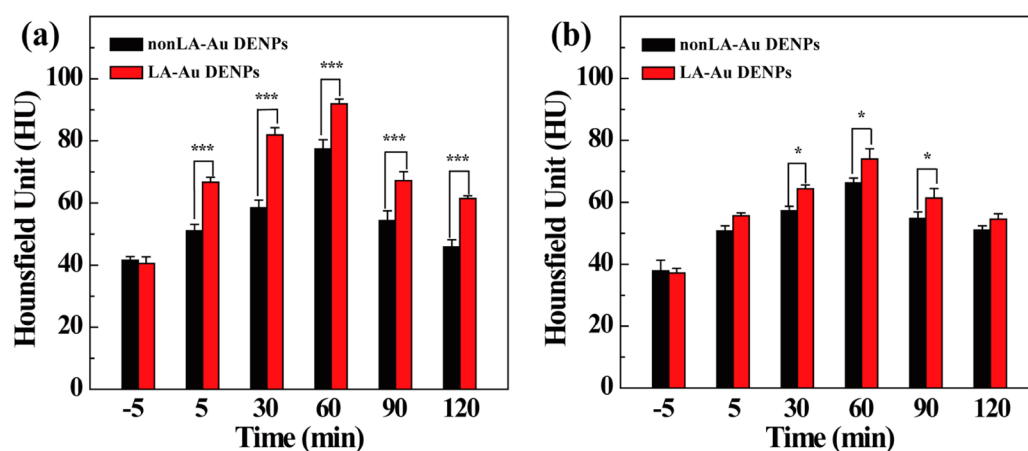
Figure 9. X-ray attenuation intensity (HU) of the tumor region before and after intravenous (a) and intraperitoneal (b) injection of nonLA-Au DENPs and LA-Au DENPs.

injected with the LA-Au DENPs are much greater than those of the nontargeted group at the same time points. Our results clearly suggest that in addition to the passive targeting effect based on EPR the active LA-mediated targeting of the tumor cells overexpressing ASGPR enables more significantly enhanced tumor CT imaging. Furthermore, compared to intraperitoneal injection (Figure 9b), intravenous injection (Figure 9a) enabled much more sensitive CT imaging of the tumor model. Lastly, the tumor CT value was also measured after intratumoral injection of Au DENPs with or without LA (Figure S5, Supporting Information). It can be clearly seen that with the time post injection of either LA-Au DENPs or nonLA-Au DENPs the tumor CT value decreases due to the tissue diffusion of the particles. However, the decreasing trend for LA-Au DENPs is much slower than that for nonLA-Au DENPs, suggesting that the targeted LA-Au DENPs are able to be retained in the tumor site for a longer time. Our data further highlighted the importance of LA-mediated active targeting, consistent with previous data reported in our group.[47] It is worth noting that ASGPR is present on the surface of both hepatocellular carcinoma cells and normal hepatocytes. Theoretically, LA-modified NPs can be uptaken by both cell lines through the receptor-mediated pathway. However, the ASGPR-expressing hepatocellular carcinoma cells are more active in endocytosis of the LA-modified NPs than the normal hepatocytes.[57] In addition, the PEGylation modification of the Au DENPs or other NPs is also beneficial to reduce the nonspecific liver uptake.[8,58,59] Therefore, the designed LA-modified Au DENPs should be promising for further biomedical applications.

ICP-OES was used to study the in vivo Au element biodistribution in major organs of mice such as the heart, liver, spleen, lung, kidney, and tumor (Figure S6, Supporting Information). It can be seen that the majority of the Au element is accumulated in the liver, spleen, and lung at 120 min post administration of both targeted and nontargeted Au DENPs. The Au uptake in the kidney, liver, and spleen for the nontargeted group is higher than that for the targeted group, which is likely owing to a quicker removal of nonLA-Au DENPs than that of the LA-Au DENPs in the reticuloendothelial system. Importantly, the tumor uptake of Au for LA-targeted Au DENPs was higher than that for nontargeted Au DENPs, further demonstrating the specific tumor targeting of LA-modified Au DENPs through a receptor-mediated manner.

From Figure S6 (Supporting Information), we can also see that the Au uptake in the kidney is comparable to that of the heart and lung, suggesting that the Au DENPs can be excreted from the body through the urinary system. To further confirm this, we measured the CT value of the bladder at different time points (Figure S7, Supporting Information). It can be clearly seen that the bladder CT value of mice injected with either nonLA-Au DENPs or LA-Au DENPs displays an increasing trend, suggesting that the Au DENPs are capable of being enriched in the bladder and that part of the particles has been excreted from the body through the urinary system in the studied time period.

CONCLUSION

To conclude, we have developed a new strategy to fabricate LA-modified Au DENPs for targeted CT imaging of human hepatocellular carcinoma. The combination of the versatile dendrimer nanotechnology with PEGylation conjugation chemistry enables the fabrication of LA-targeted Au DENPs with good stability under varying pH and temperature conditions and in different aqueous media. The formed LA-Au DENPs show satisfactory cytocompatibility in the given concentration range to normal cells. In vitro flow cytometry results reveal that the LA-Au DENPs are able to specifically target human hepatocellular carcinoma cells (HepG2 cells) through the receptor-mediated active targeting pathway. The LA-modified Au DENPs with good X-ray attenuation property can be used as an efficient nanoprobe for targeted CT imaging of human hepatocellular carcinoma in vitro and the xenografted tumor model in vivo. With the ability to be further functionalized with anticancer drugs and different biological ligands, the developed Au DENP-based nanoplatform should be promising for cancer theranostics applications.

ASSOCIATED CONTENT

Ⓢ Supporting Information

Additional materials characterization and in vivo evaluation data. This material is available free of charge via the Internet at http://pubs.acs.org.

AUTHOR INFORMATION

Corresponding Authors
*E-mail: xshi@dhu.edu.cn
*E-mail: guixiangzhang@sina.com

*E-mail: mwshen@dhu.edu.cn.

Author Contributions

[⊥]These authors contributed equally to this work.

Notes

The authors declare no competing financial interest.

■ REFERENCES

(1) Villanueva, A.; Llovet, J. M. Targeted Therapies for Hepatocellular Carcinoma. *Gastroenterology* **2011**, *140*, 1410−1426.

(2) Liu, Y. J.; Chen, Z. J.; Liu, C. X.; Yu, D. X.; Lu, Z. J.; Zhang, N. Gadolinium-loaded Polymeric Nanoparticles Modified with Anti-VEGF as Multifunctional MRI Contrast Agents for the Diagnosis of Liver Cancer. *Biomaterials* **2011**, *32*, 5167−5176.

(3) Wang, H.; Zheng, L.; Peng, C.; Shen, M.; Shi, X.; Zhang, G. Folic Acid-Modified Dendrimer-Entrapped Gold Nanoparticles as Nanoprobes for Targeted CT Imaging of Human Lung Adencarcinoma. *Biomaterials* **2013**, *34*, 470−480.

(4) Mankoff, D. A. A Definition of Molecular Imaging. *J. Nucl. Med.* **2007**, *48*, 18N−21N.

(5) Lusic, H.; Grinstaff, M. W. X-Ray-Computed Tomography Contrast Agents. *Chem. Rev.* **2012**, *113*, 1641−1666.

(6) Jakhmola, A.; Anton, N.; Vandamme, T. Inorganic Nanoparticles Based Contrast Agents for X-Ray Computed Tomography. *Adv. Healthcare Mater.* **2012**, *1*, 413−431.

(7) Kim, D. K.; Park, S. J.; Lee, J. H.; Jeong, Y. Y.; Jon, S. Y. Antibiofouling Polymer-Coated Gold Nanoparticles as a Contrast Agent for in vivo X-Ray Computed Tomography Imaging. *J. Am. Chem. Soc.* **2007**, *129*, 7661−7665.

(8) Peng, C.; Zheng, L.; Chen, Q.; Shen, M.; Guo, R.; Wang, H.; Cao, X.; Zhang, G.; Shi, X. PEGylated Dendrimer-Entrapped Gold Nanoparticles for in vivo Blood Pool and Tumor Imaging by Computed Tomography. *Biomaterials* **2012**, *33*, 1107−1119.

(9) Reuveni, T.; Motiei, M.; Romman, Z.; Popovtzer, A.; Popovtzer, R. Targeted Gold Nanoparticles Enable Molecular CT Imaging of Cancer: An in vivo Study. *Int. J. Nanomed.* **2011**, *6*, 2859−2864.

(10) Guo, R.; Wang, H.; Peng, C.; Shen, M.; Zheng, L.; Zhang, G.; Shi, X. Enhanced X-Ray Attenuation Property of Dendrimer-Entrapped Gold Nanoparticles Complexed with Diatrizoic Acid. *J. Mater. Chem.* **2011**, *21*, 5120−5127.

(11) Ai, K. L.; Liu, Y. L.; Liu, J. H.; Yuan, Q. H.; He, Y. Y.; Lu, L. H. Large-Scale Synthesis of Bi2S3 Nanodots as a Contrast Agent for in vivo X-Ray Computed Tomography Imaging. *Adv. Mater.* **2011**, *23*, 4886−4891.

(12) Hainfeld, J. F.; Slatkin, D. N.; Focella, T. M.; Smilowitz, H. M. Gold Nanoparticles: A New X-Ray Contrast Agent. *Br. J. Radiol.* **2006**, *79*, 248−253.

(13) Hallouard, F.; Anton, N.; Choquet, P.; Constantinesco, A.; Vandamme, T. Iodinated Blood Pool Contrast Media for Preclinical X-Ray Imaging Applications-A Review. *Biomaterials* **2010**, *31*, 6249−6268.

(14) Rigsby, C. K.; Gasber, E.; Seshadri, R.; Sullivan, C.; Wyers, M.; Ben-Ami, T. Safety and Efficacy of Pressure-Limited Power Injection of Iodinated Contrast Medium through Central Lines in Children. *Am. J. Roentgenol.* **2007**, *188*, 726−732.

(15) Fang, Y.; Peng, C.; Guo, R.; Zheng, L.; Qin, J.; Zhou, B.; Shen, M.; Lu, X.; Zhang, G.; Shi, X. Dendrimer-Stabilized Bismuth Sulfide Nanoparticles: Synthesis, Characterization, and Potential Computed Tomography Imaging Applications. *Analyst* **2013**, *138*, 3172−3180.

(16) Rabin, O.; Perez, J. M.; Grimm, J.; Wojtkiewicz, G.; Weissleder, R. An X-Ray Computed Tomography Imaging Agent Based on Long-Circulating Bismuth Sulphide Nanoparticles. *Nat. Mater.* **2006**, *5*, 118−122.

(17) Liu, Y. L.; Ai, K. L.; Liu, J. H.; Yuan, Q. H.; He, Y. Y.; Lu, L. H. A High-Performance Ytterbium-Based Nanoparticulate Contrast Agent for in vivo X-Ray Computed Tomography Imaging. *Angew. Chem., Int. Ed.* **2012**, *51*, 1437−1442.

(18) Popovtzer, R.; Agrawal, A.; Kotov, N. A.; Popovtzer, A.; Balter, J.; Carey, T. E.; Kopelman, R. Targeted Gold Nanoparticles Enable Molecular CT Imaging of Cancer. *Nano Lett.* **2008**, *8*, 4593−4596.

(19) Regino, C. A. S.; Walbridge, S.; Bernardo, M.; Wong, K. J.; Johnson, D.; Lonser, R.; Oldfield, E. H.; Choyke, P. L.; Brechbiel, M. W. A Dual CT-MR Dendrimer Contrast Agent as a Surrogate Marker for Convection-Enhanced Delivery of Intracerebral Macromolecular Therapeutic Agents. *Contrast Media Mol. Imaging* **2008**, *3*, 2−8.

(20) McDonald, M. A.; Watkin, K. L. Small Particulate Gadolinium Oxide and Gadolinium Oxide Albumin Microspheres as Multimodal Contrast and Therapeutic Agents. *Invest. Radiol.* **2003**, *38*, 305−310.

(21) Liu, H.; Xu, Y.; Wen, S.; Zhu, J.; Zheng, L.; Shen, M.; Zhao, J.; Zhang, G.; Shi, X. Facile Formation of Low Generation Dendrimer-Stabilized Gold Nanoparticles for in vivo X-Ray Computed Tomography Imaging Applications. *Polym. Chem.* **2013**, *4*, 1788−1795.

(22) Wang, H.; Zheng, L.; Peng, C.; Guo, R.; Shen, M.; Shi, X.; Zhang, G. Computed Tomography Imaging of Cancer Cells Using Acetylated Dendrimer-Entrapped Gold Nanoparticles. *Biomaterials* **2011**, *32*, 2979−2988.

(23) Cormode, D. P.; Roessl, E.; Thran, A.; Skajaa, T.; Gordon, R. E.; Schlomka, J.-P.; Fuster, V.; Fisher, E. A.; Mulder, W. J. M.; Proksa, R.; Fayad, Z. A. Atherosclerotic Plaque Composition: Analysis with Multicolor CT and Targeted Gold Nanoparticles. *Radiology* **2010**, *256*, 774−782.

(24) Sun, I.-C.; Eun, D.-K.; Na, J. H.; Lee, S.; Kim, I.-J.; Youn, I.-C.; Ko, C.-Y.; Kim, H.-S.; Lim, D.; Choi, K.; Messersmith, P. B.; Park, T. G.; Kim, S. Y.; Kwon, I. C.; Kim, K.; Ahn, C.-H. Heparin-Coated Gold Nanoparticles for Liver-Specific CT Imaging. *Chem.—Eur. J.* **2009**, *15*, 13341−13347.

(25) Wen, S.; Li, K.; Cai, H.; Chen, Q.; Shen, M.; Huang, Y.; Peng, C.; Hou, W.; Zhu, M.; Zhang, G.; Shi, X. Multifunctional Dendrimer-Entrapped Gold Nanoparticles for Dual Mode CT/MR Imaging Applications. *Biomaterials* **2013**, *34*, 1570−1580.

(26) Guo, R.; Wang, H.; Peng, C.; Shen, M.; Pan, M.; Cao, X.; Zhang, G.; Shi, X. X-Ray Attenuation Property of Dendrimer-Entrapped Gold Nanoparticles. *J. Phys. Chem. C* **2010**, *114*, 50−56.

(27) Li, D. X.; He, Q.; Li, J. B. Smart Core/shell Nanocomposites: Intelligent Polymers Modified Gold Nanoparticles. *Adv. Colloid Interface Sci.* **2009**, *149*, 28−38.

(28) Li, D. X.; Cui, Y.; Wang, K. W.; He, Q.; Yan, X. H.; Li, J. B. Thermosensitive Nanostructures Comprising Gold Nanoparticles Grafted with Block Copolymers. *Adv. Funct. Mater.* **2007**, *17*, 3134−3140.

(29) Li, D. X.; He, Q.; Cui, Y.; Li, J. B. Fabrication of pH-Responsive Nanocomposites of Gold Nanoparticles/Poly(4-Vinylpyridine). *Chem. Mater.* **2007**, *19*, 412−417.

(30) Li, D. X.; He, Q.; Cui, Y.; Wang, K. W.; Zhang, X. M.; Li, J. B. Thermosensitive Copolymer Networks Modify Gold Nanoparticles for Nanocomposite Entrapment. *Chem.—Eur. J.* **2007**, *13*, 2224−2229.

(31) Li, D. X.; Li, C. F.; Wang, A. H.; He, Q.; Li, J. B. Hierarchical Gold/Copolymer Nanostructures as Hydrophobic Nanotanks for Drug Encapsulation. *J. Mater. Chem.* **2010**, *20*, 7782–7787.

(32) Li, D. X.; He, Q.; Yang, Y.; Möhwald, H.; Li, J. B. Two-Stage pH Response of Poly(4-vinylpyridine) Grafted Gold Nanoparticles. *Macromolecules* **2008**, *41*, 7254–7256.

(33) Li, D. X.; Li, C. F.; Yang, Y.; He, Q.; Li, J. B. Interfacial Dispersion of Poly(N-isopropylacrylamide)/Gold Nanocomposites. *J. Nanosci. Nanotechnol.* **2011**, *11*, 2052–2056.

(34) Gao, L.; Fei, J. B.; Zhao, J.; Li, H.; Cui, Y.; Li, J. B. Hypocrellin-Loaded Gold Nanocages with High Two-Photon Efficiency for Photothermal/Photodynamic Cancer Therapy in Vitro. *ACS Nano* **2012**, *6*, 8030–8040.

(35) Shukla, R.; Hill, E.; Shi, X.; Kim, J.; Muniz, M. C.; Sun, K.; Baker, J. R., Jr. Tumor Microvasculature Targeting with Dendrimer-Entrapped Gold Nanoparticles. *Soft Matter* **2008**, *4*, 2160–2163.

(36) Shi, X.; Wang, S. H.; Van Antwerp, M. E.; Chen, X.; Baker, J. R., Jr. Targeting and Detecting Cancer Cells using Spontaneously Formed Multifunctional Dendrimer-Stabilized Gold Nanoparticles. *Analyst* **2009**, *134*, 1373–1379.

(37) Shi, X.; Wang, S. H.; Meshinchi, S.; Van Antwerp, M. E.; Bi, X.; Lee, I.; Baker, J. R., Jr. Dendrimer-Entrapped Gold Nanoparticles as a Platform for Cancer-Cell Targeting and Imaging. *Small* **2007**, *3*, 1245–1252.

(38) Shen, M.; Shi, X. Dendrimer-Based Organic/Inorganic Hybrid Nanoparticles in Biomedical Applications. *Nanoscale* **2010**, *2*, 1027–1032.

(39) Peng, C.; Qin, J.; Zhou, B.; Chen, Q.; Shen, M.; Zhu, M.; Lu, X.; Shi, X. Targeted Tumor CT Imaging Using Folic Acid-Modified PEGylated Dendrimer-Entrapped Gold Nanoparticles. *Polym. Chem.* **2013**, *4*, 4412–4424.

(40) Zheng, L.; Zhu, J.; Shen, M.; Chen, X.; Baker, J. R., Jr.; Wang, S. H.; Zhang, G.; Shi, X. Targeted Cancer Cell Inhibition Using Multifunctional Dendrimer-Entrapped Gold Nanoparticles. *Med. Chem. Commun.* **2013**, *4*, 1001–1005.

(41) Bronstein, L. M.; Shifrina, Z. B. Dendrimers as Encapsulating, Stabilizing, or Directing Agents for Inorganic Nanoparticles. *Chem. Rev.* **2011**, *111*, 5301–5344.

(42) Mintzer, M. A.; Grinstaff, M. W. Biomedical Applications of Dendrimers: A Tutorial. *Chem. Soc. Rev.* **2011**, *40*, 173–190.

(43) Xiao, T.; Wen, S.; Wang, H.; Liu, H.; Shen, M.; Zhao, J.; Zhang, G.; Shi, X. Facile Synthesis of Acetylated Dendrimer-Entrapped Gold Nanoparticles with Enhanced Gold Loading for CT Imaging Applications. *J. Mater. Chem. B* **2013**, *1*, 2773–2780.

(44) Peng, C.; Li, K.; Cao, X.; Xiao, T.; Hou, W.; Zheng, L.; Guo, R.; Shen, M.; Zhang, G.; Shi, X. Facile Formation of Dendrimer-Stabilized Gold Nanoparticles Modified with Diatrizoic Acid for Enhanced Computed Tomography Imaging Applications. *Nanoscale* **2012**, *4*, 6768–6778.

(45) Shi, X.; Sun, K.; Baker, J. R., Jr. Spontaneous Formation of Functionalized Dendrimer-Stabilized Gold Nanoparticles. *J. Phys. Chem. C* **2008**, *112*, 8251–8258.

(46) Liu, H.; Xu, Y.; Wen, S.; Chen, Q.; Zheng, L.; Shen, M.; Zhao, J.; Zhang, G.; Shi, X. Targeted Tumor Computed Tomography Imaging Using Low Generation Dendrimer-Stabilized Gold Nanoparticles. *Chem.—Eur. J.* **2013**, *19*, 6409–6416.

(47) Chen, Q.; Li, K.; Wen, S.; Liu, H.; Peng, C.; Cai, H.; Shen, M.; Zhang, G.; Shi, X. Targeted CT/MR Dual Mode Imaging of Tumors Using Multifunctional Dendrimer-Entrapped Gold Nanoparticles. *Biomaterials* **2013**, *34*, 5200–5209.

(48) Ashwell, G.; Harford, J. Carbohydrate-Specific Receptors of the Liver. *Annu. Rev. Biochem.* **1982**, *51*, 531–554.

(49) Schwartz, A. L.; Fridovich, S. E.; Knowles, B. B.; Lodish, H. F. Characterization of the Asialoglycoprotein Receptor in a Continuous Hepatoma Line. *J. Biol. Chem.* **1981**, *256*, 8878–8881.

(50) Guo, R.; Yao, Y.; Cheng, G.; Wang, S. H.; Li, Y.; Shen, M.; Zhang, Y.; Baker, J. R., Jr.; Wang, J.; Shi, X. Synthesis of Glycoconjugated Poly(amindoamine) Dendrimers for Targeting Human Liver Cancer Cells. *RSC Adv.* **2012**, *2*, 99–102.

(51) Medina, S. H.; Tekumalla, V.; Chevliakov, M. V.; Shewach, D. S.; Ensminger, W. D.; El-Sayed, M. E. H. N-Acetylgalactosamine-Functionalized Dendrimers as Hepatic Cancer Cell-Targeted Carriers. *Biomaterials* **2011**, *32*, 4118–4129.

(52) Soenen, S. J. H.; Brisson, A. R.; Jonckheere, E.; Nuytten, N.; Tan, S.; Himmelreich, U.; De Cuyper, M. The Labeling of Cationic Iron Oxide Nanoparticle-Resistant Hepatocellular Carcinoma Cells Using Targeted Magnetoliposomes. *Biomaterials* **2011**, *32*, 1748–1758.

(53) Wang, Y.; Guo, R.; Cao, X.; Shen, M.; Shi, X. Encapsulation of 2-Methoxyestradiol within Multifunctional Poly(amidoamine) Dendrimers for Targeted Cancer Therapy. *Biomaterials* **2011**, *32*, 3322–3329.

(54) Shi, X.; Wang, S. H.; Sun, H.; Baker, J. R., Jr. Improved Biocompatibility of Surface Functionalized Dendrimer-Entrapped Gold Nanoparticles. *Soft Matter* **2007**, *3*, 71–74.

(55) Shi, X.; Wang, S. H.; Swanson, S. D.; Ge, S.; Cao, Z.; Van Antwerp, M. E.; Landmark, K. J.; Baker, J. R., Jr. Dendrimer-Functionalized Shell-Crosslinked Iron Oxide Nanoparticles for in vivo Magnetic Resonance Imaging of Tumors. *Adv. Mater.* **2008**, *20*, 1671–1678.

(56) Liu, H.; Shen, M.; Zhao, J.; Guo, R.; Cao, X.; Zhang, G.; Shi, X. Tunable Synthesis and Acetylation of Dendrimer-Entrapped or Dendrimer-Stabilized Gold–Silver Alloy Nanoparticles. *Colloids Surf., B* **2012**, *94*, 58–67.

(57) Medina, S. H.; Tiruchinapally, G.; Chevliakov, M. V.; Durmaz, Y. Y.; Stender, R. N.; Ensminger, W. D.; Shewach, D. S.; ElSayed, M. E. H. Targeting hepatic cancer cells with PEGylated dendrimers displaying N-acetylgalactosamine and SP94 peptide ligands. *Adv. Healthcare Mater.* **2013**, *2*, 1337–1350.

(58) Cai, H.; An, X.; Cui, J.; Li, J.; Wen, S.; Li, K.; Shen, M.; Zheng, L.; Zhang, G.; Shi, X. Facile hydrothermal synthesis and surface functionalization of polyethyleneimine-coated iron oxide nanoparticles for biomedical applications. *ACS Appl. Mater. Interfaces* **2013**, *5*, 1722–1731.

(59) Li, J.; Zheng, L.; Cai, H.; Sun, W.; Shen, M.; Zhang, G.; Shi, X. Polyethyleneimine-mediated synthesis of folic acid-targeted iron oxide nanoparticles for *in vivo* tumor MR imaging. *Biomaterials* **2013**, *34*, 8382–8392.